Remote Changes in the Dynamics of the Phosphotyrosine-Binding Domain of Insulin Receptor Substrate-1 Induced by Phosphopeptide Binding[†]

Virginia A. Jarymowycz[‡] and Martin J. Stone*[,§]

Department of Chemistry and Interdisciplinary Biochemistry Program, Indiana University, Bloomington, Indiana 47405-0001, and Department of Biochemistry and Molecular Biology, Monash University, Clayton, VIC 3800, Australia

Received June 10, 2008; Revised Manuscript Received October 27, 2008

ABSTRACT: Protein structures consist of cooperative networks of interactions that can extend substantial distances across the protein structure and have significant consequences for stability and function. To characterize such interaction networks within the phosphotyrosine-binding domain of insulin receptor substrate-1 (IRS-PTB), we have used NMR relaxation to determine the dynamics of backbone amide groups, side chain methyl groups, and tryptophan side chain indole groups in IRS-PTB, both in the absence and in the presence of a bound phosphotyrosine-containing peptide. Although there are minimal differences between the structures of apo and peptide-bound forms, primarily localized close to the peptide binding site, we observe significant changes in dynamics for residues located remotely from the binding site. These residues are clustered together and appear to constitute a network of interactions that is coupled to the peptide binding site through intervening residues.

Folded protein structures are generally understood to consist of cooperative networks of interactions. This property of proteins suggests that the formation or breakage of interactions at one position in a protein could potentially influence the interactions at positions remote from the modification. Indeed, the existence of such "long-range communication" between distant amino acid residues is supported by both experimental and computational evidence. Experimentally, it is not uncommon to find mutations that have substantial effects on the function of a protein despite being in regions distant from the active site. Examples include the influence of distal mutations on the hydride transfer kinetics of dihydrofolate reductase (*1*) and on the enanteoselectivity of the *Pseudomonas aeruginosa* lipase (*2*). In addition, double mutant cycle experiments have shown that spatially separated mutations often have nonadditive effects on the stability of a protein (*3, 4*); in one recent study of 120 nonadjacent mutant pairs in a variety of proteins, more than 40% were found to exhibit nonadditive influences on stability (*5*). The experimental evidence for long-range networks is corroborated by computational and bioinformatic approaches. Molecular dynamics simulations of dihydrofolate reductase predict the aforementioned influence of distal mutations on catalytic activity (*6*). Similarly, statistical correlation analysis (SCA), a bioinformatic method for analyzing evolutionary covariation, has demonstrated that amino acids separated by considerable distances within a structure can exert evolutionary selection pressure on each other with consequences for both protein stability and function (*7*); predictions based on SCA results have been experimentally verified (*8, 9*).

To understand the mechanism by which remote residues can influence each other, it is necessary to identify the network(s) of intervening residues through which they communicate. Long-range interactions have been suggested to involve correlations between the motions of the distantly located residues (*6*). Therefore, one approach is to study the dynamical properties of the protein. Amino acid backbone and side chain groups within proteins are constantly fluctuating on very fast time scales (picoseconds to nanoseconds). Analysis of NMR[1] relaxation data provides information about the spatial restriction of these fluctuations (reviewed by V. A. Jarymowycz and M. J. Stone in 2006), which is related to the partition function (the distribution of energy states) for the fluctuating group. Thus, modification of specific interactions (through mutagenesis or ligand binding) could potentially lead to changes in the dynamics of groups throughout the relevant network of interactions, and these changes could be detected by NMR. This perturbation-based approach has been applied previously by Lee and co-workers who investigated the effects of peptide binding on the dynamics of the second PDZ domain (PDZ2) of human protein tyrosine phosphatase 1E (hPTP1E) (*10*) and mutational perturbation upon the dynamics of serine protease inhibitor eglin c (*11, 12*). In each case, the perturbations

[†] This work was supported by a grant awarded to M.J.S. from the National Science Foundation (MCB-0212746) and by the Baxter Pharmaceutical Fellowship awarded to V.A.J.

* To whom correspondence should be addressed: Department of Biochemistry and Molecular Biology, Monash University, Clayton, VIC 3800, Australia. Phone: +61-3-9905-5937. Fax: +61-3-9905-3726. E-mail: martin_stone@med.monash.edu.au.

[‡] Indiana University.

[§] Monash University.

[1] Abbreviations: η_{xy}, cross-relaxation rate constant; HSQC, heteronuclear single-quantum coherence; IRS-1, insulin receptor substrate-1; IRS-PTB, phosphotyrosine-binding domain of insulin receptor substrate-1; NMR, nuclear magnetic resonance; NOE, nuclear Overhauser effect; PTB, phosphotyrosine-binding domain; R_1, longitudinal relaxation rate constant; R_2, transverse relaxation rate constant; R_{ex}, conformational exchange rate; S^2, order parameter; τ_e, internal correlation time; τ_m, rotational correlation time.

10.1021/bi801096b CCC: $40.75
Published on Web 11/17/2008

resulted in substantial changes in the fast dynamics of side chain methyl groups, with many of the residues exhibiting these changes forming contiguous pathways extending to points 9−16 Å from the nearest residue in the peptide ligand or mutation site.

This paper describes an NMR study of long-range dynamical effects in the phosphotyrosine-binding domain (PTB) of insulin receptor substrate-1 (IRS-1), hereafter termed IRS-PTB. IRS-1 mediates insulin signaling by functioning as a scaffold that links the activated insulin receptor or interleukin-4 (IL-4) receptor to downstream effector proteins (*13, 14*). IRS-1 is composed of an N-terminal plekstrin homology (PH) domain, the PTB, and several tyrosine phosphorylation motifs. Upon receptor activation and autophosphorylation, the PTB binds to a phosphorylated receptor tyrosine residue (*15*), rendering IRS-1 a substrate for tyrosine phosphorylation catalyzed by the receptor. The phosphorylated tyrosine motifs of IRS-1 then recruit signaling proteins that contain SH2 domains (*13, 14*). The PH domain of IRS-1 facilitates interaction with the receptors by targeting the protein to the membrane through binding of membrane phospholipids (*14*). A study of IRS-PTB in isolation has found that this domain may also function to bind membrane phospholipids using a face of the domain unique from that of the phosphotyrosine binding site (*16*), although a separate study observed no binding of inositol phosphate or phosphoinositides by IRS-PTB (*17*).

The three-dimensional structure of IRS-PTB is extremely similar in the apo state and bound to a phosphopeptide derived from the IL-4 receptor; Cα atoms of core residues superimpose with a root-mean-square deviation (rmsd) of 0.29 Å (*18*). The structure consists of a β-sandwich and a long C-terminal α-helix, and the peptide binds in a cleft formed by the helix and the edge of one β-sheet. A previous NMR study by Olejniczak et al. (*19*) indicated that binding of the same phosphopeptide induces changes in the backbone dynamics of IRS-PTB at positions distant from the peptide binding site. Thus, the question of how the remote residues sense the presence of the peptide arises, i.e., whether a network of transient interactions or coupled motions exists. In light of recent technological and methodological advances in NMR data collection and analysis, we have re-examined the backbone fluctuations of IRS-PTB and have also determined the fluctuations of both side chain methyl groups and tryptophan indole groups in the apo and phosphopeptide-bound states. Herein, we describe the results and discuss their implications for a network of dynamical interactions extending across IRS-PTB.

MATERIALS AND METHODS

Sample Preparation. A gene construct encoding residues 157−278 of IRS-1 with a Gly residue inserted between residues 267 and 268 and an additional Leu-Glu-$(His)_6$ motif at the C-terminus was synthesized on the basis of a previously published sequence (*20*) using recursive PCR. The Gly insertion gives rise to a modified thrombin cleavage site (FRPR-GS vs the canonical LVPR-GS), allowing the desired protein to be obtained by thrombin cleavage of the expressed protein (vide infra). The sequence of the IRS-PTB gene construct is given in the Supporting Information. The gene construct was subcloned into a pET30a vector (Novagen, Madison, WI), and the recombinant vector was transformed into BL21(DE3) cells (Novagen). Cells were grown in LB medium at 20 °C. When an optical density (600 nm) of ∼0.55 was reached, isopropyl β-D-thiogalactopyranoside (IPTG) was added to a final concentration of 200 μM. The cells were harvested 18 h after induction by centrifugation. Cells were resuspended in ∼20 mL of 20 mM Tris-HCl, 5 mM imidazole, and 500 mM NaCl (pH 7.8) per liter of growth medium and lysed by sonication. The cell lysate was centrifuged at 15000 rpm for 30 min at 4 °C, and the supernatant was filtered using a 0.2 μm filter. The filtered supernatant was purified by Ni^{2+} affinity chromatography using Ni-NTA agarose (Qiagen) and wash and elution buffers containing 20 mM Tris-HCl, 500 mM NaCl (pH 7.8), and 20 and 200 mM imidazole, respectively, according to the manufacturer's instructions. Eluted IRS-1 was dialyzed against 20 mM BisTris, 250 mM NaCl, 25 mM $CaCl_2$, and 5 mM BME (pH 6.5) for ∼16 h at 4 °C. Subsequently, IRS-1 was incubated with 17 units of thrombin per milligram of protein for ∼20 h at 25 °C. Thrombin cleavage of IRS-1 at the modified cleavage site, yielding IRS-PTB (residues 157−267), was monitored by SDS−PAGE analysis. IRS-PTB was purified from uncleaved IRS-1 by Ni^{2+} affinity chromatography and further purified by size exclusion chromatography using a HiPrep 16/60 Sephacryl S-100 HR column (Amersham Biosciences). The final identity and purity of IRS-PTB were determined by MALDI-TOF mass spectrometry and SDS−PAGE analysis, respectively. Protein concentrations were determined from the absorbance at 280 nm using an extinction coefficient of 12615 L mol^{-1} cm^{-1}, calculated from the domain's amino acid sequence (*21*). In a modification to this protocol, samples prepared for backbone amide dynamics experiments were grown in M9 minimal medium containing 3.0 g/L KH_2PO_4, 0.5 g/L NaCl, 6.0 g/L Na_2HPO_4, 2.0 g/L glucose, and 1.0 g/L $^{15}NH_4Cl$. Samples prepared for side chain methyl dynamics experiments were grown in M9 minimal medium containing 2.0 g/L [$^{13}C_6$]glucose, 3.0 g/L KH_2PO_4, 0.5 g/L NaCl, 6.0 g/L Na_2HPO_4, 1.0 g/L $^{15}NH_4Cl$, and a D_2O:H_2O ratio of 3:2. Samples prepared for stereospecific assignment of valine $C_\gamma H_3$ and leucine $C_\delta H_3$ resonances were grown in M9 minimal medium used for ^{15}N isotopic labeling but modified to contain 10% [$^{13}C_6$]glucose and 90% natural abundance glucose (*22*).

A tyrosine-phosphorylated peptide derived from the IL-4 receptor (LVIAGNPApYRS) was synthesized using solid phase methods and purified using HPLC with a C18 semipreparative column (Vydac). The identity of the peptide was confirmed by MALDI-TOF mass spectrometry, and the purity was estimated by HPLC to be >95%. The peptide was lyophilized and resuspended in water. The peptide concentration was determined by amino acid analysis (AAA Service Laboratory, Boring, OR). A complex between IRS-PTB and the IL-4 receptor peptide (K_d = 6 μM as previously measured using isothermal titration calorimetry) (*20*) was formed by addition of peptide under the same buffer conditions to the protein which yielded a stoichiometery of 1:1.5 (protein:peptide).

NMR Measurements. All NMR spectra were acquired from samples consisting of isotopically labeled PTB of IRS in 20 mM BisTris, 50 mM NaCl, 5 mM DTT, and a H_2O:D_2O ratio of 9:1 (pH 6.5) at 30 °C on a Varian NMR Systems

600 MHz NMR spectrometer equipped with four radiofrequency channels and a triple-resonance Cold Probe.

Sequential resonance assignments of the backbone amide ^{1}H and ^{15}N atoms were obtained from three-dimensional (3D) HNCACB and CBCACONH spectra (*23*−*25*). The ^{1}H carrier was placed on the water resonance; the ^{13}C carrier was placed at 46 ppm, and the ^{15}N carrier was placed at 119 ppm. The experiments were conducted using 2048, 64, and 32 complex points and spectral widths of 8446, 10856, and 1840 Hz in the ^{1}H, ^{13}C, and ^{15}N dimensions, respectively. Ambiguities in assignments were resolved using 3D TOCSY-HSQC and NOESY-HSQC spectra (*26*), in which the ^{1}H and ^{15}N carrier frequencies were the same as stated above and the experiments were conducted using 2048, 192, and 32 complex points and spectral widths of 8446, 7799, and 1840 Hz in the ^{1}H, direct ^1H_N, and ^{15}N dimensions, respectively. Resonance assignments of side chain methyl ^{1}H and ^{13}C atoms were obtained from 3D C(CO)NH TOCSY and H(CCO)NH TOCSY spectra (*27, 28*), in which the ^{1}H and ^{13}C carriers were the same as stated above and the experiments were conducted using 2048, 64, 64, and 32 complex points and spectral widths of 8446, 10856, 7496, and 1840 Hz in the ^{1}H, ^1H_C, ^{13}C, and ^{15}N dimensions, respectively. Additionally, methyl ^{1}H and ^{13}C resonance assignments were obtained from HCCH-TOCSY spectra (*29*), in which the ^{1}H and ^{13}C carriers were the same as stated above and the experiments were conducted using 2048, 64, and 32 complex points and spectral widths of 7225, 7225, and 10858 Hz in the destination ^{1}H, origin ^{1}H, and origin ^{13}C dimensions, respectively. Stereospecific methyl ^{1}H and ^{13}C resonance assignments for leucine and valine residues were obtained using a fractional [^{13}C]glucose labeling method (*22*). Methionine methyl resonance assignments were obtained from 3D LRCC experiments (*30*), in which the ^{1}H and ^{13}C carriers were the same as stated above and the experiments were conducted using 2048, 96, and 32 complex points and spectral widths of 7225, 10858, and 3016 Hz in the destination ^{1}H, $^{13}C_{\varepsilon\gamma\beta}$, and $^{13}C_{\varepsilon}$ dimensions, respectively. Assigned ^{1}H−^{15}N and ^{1}H−^{13}C HSQC spectra are given in the Supporting Information. Resonance assignments have been deposited with BMRB (accession number 15959).

Backbone amide and tryptophan side chain indole ^{15}N longitudinal relaxation rate constants (R_1), ^{15}N transverse relaxation rate constants (R_2), {^{1}H}−^{15}N steady-state nuclear Overhauser enhancements (NOE), and ^{15}N transverse cross-relaxation rate constants (η_{xy}) were measured using published two-dimensional (2D) ^{1}H−^{15}N HSQC-style pulse sequences (*31*−*33*). The ^{1}H carrier was placed on the water resonance, and the ^{15}N carrier was placed at 119 ppm. For the R_1 experiments, the following delays (τ) were used: 0.01*, 0.03, 0.08, 0.13*, 0.25, 0.40*, 0.65, and 1.00* ms. For the R_2 experiments, the following delays (τ) were used: 0.01*, 0.03, 0.05*, 0.07, 0.11, 0.15*, 0.19, and 0.25* ms. Asterisks indicate delays at which data were collected in duplicate to allow estimation of uncertainties in peak heights. NOE spectra were recorded in duplicate. All experiments were conducted using 2048 and 128 complex points and spectral widths of 10000 and 1840 Hz in the ^{1}H and ^{15}N dimensions, respectively.

Side chain methyl group (CH_2D) deuterium longitudinal relaxation rate constants (R_1) and deuterium transverse relaxation rate constants ($R_{1\rho}$) were measured using published 2D ^{1}H−^{13}C HSQC-style pulse sequences (*34*). The ^{1}H carrier was placed on the water resonance, and the ^{13}C carrier was placed at 20 ppm. The relaxation delay (τ) was varied among nine different times. At four of these times, experiments were duplicated to estimate peak height uncertainty. For the R_1 experiments, the following delays (τ) were used: 0.05*, 5, 10, 15, 21*, 28, 36*, 45, and 58* ms. For the $R_{1\rho}$ experiments, the following delays were used: 0.2*, 1.5, 4, 6.5, 9*, 12, 16*, 21, and 29* ms. Asterisks indicated delays at which data were collected in duplicate. For the $R_{1\rho}$ experiment, the shortest time point gave anomalously low peak intensities and was therefore excluded from the data analysis. All experiments were conducted using 2048 and 48 complex points and spectral widths of 6010 and 2714 Hz in the ^{1}H and ^{13}C dimensions, respectively.

Data Analysis. NMR data were processed using FELIX98 (Molecular Simulation, Inc.). Relaxation parameters and standard errors were extracted as described in ref *35*. Resonances with significant spectral overlap, weak peak intensity, or ambiguous assignments were excluded from data analyses. Backbone amide groups with large-amplitude internal motions on a picosecond time scale, as identified by characteristically low NOE values (NOE < 0.5), or with conformational exchange (R_{ex}) on a slow time scale, as identified by R_2/η_{xy} ratios deviating from the average by one standard deviation, were excluded from estimation of the overall correlation time (τ_m) and rotational diffusion tensor (*36*). Subsequently, several residues with unusually elevated R_1 values (greater than one standard deviation above the average) were also excluded from diffusion tensor estimation; all of these residues are located at the termini of the protein or near loop regions and may be subject to some dynamical effect that the core of the protein does not experience. In the free state of IRS-PTB, the following residues were excluded: 262 (low NOE); 222, 227, 241, 242, and 246 (high R_2/η_{xy} ratio); 159, 160, 171, 201, 263−265, and 267 (both low NOE value and high R_2/η_{xy} ratio); and 173−175, 178, 189, 191, 192, 198, 231, 243, and 261 (high R_1). In the bound state of IRS-PTB, the following residues were excluded: 160, 201, 263−265, and 267 (low NOE); 217, 227, and 247 (high R_2/η_{xy} ratio); 159 (both low NOE and high R_2/η_{xy} ratio); and 174, 180, 188, 191, 193, 198, 202, 208, 218, 225, 229, and 243 (high R_1). Overall correlation times and rotational diffusion tensors for isotropic, axially symmetric, and fully anisotropic models were estimated from the R_2/R_1 ratios of the remaining backbone amide groups (63 of 108 for the free state and 57 of 108 for the bound state) and the energy-minimized average NMR structure coordinates for IRS-PTB [Protein Data Bank (PDB) entry 1IRS (*20*)] using the program quadric_diffusion (A. G. Palmer, III, Columbia University, New York, NY) (*37*). The most appropriate diffusion tensor was selected by a comparison of χ^2 goodness-of-fit parameters and using *F*-statistical analysis. Using this rotational diffusion tensor, backbone relaxation data were fit to five variations of the Lipari−Szabo model-free formalism (*38*−*42*) commonly termed "models" 1−5 using ModelFree (A. G. Palmer, III) and a ^{15}N CSA value of −170 ppm. The fitted dynamics parameters for each model are as follows: model 1, order parameter (S^2); model 2, S^2 and internal correlation time (τ_e); model 3, S^2 and exchange broadening contribution to transverse relaxation (R_{ex}); model 4, S^2, τ_e, and R_{ex}; model 5, order parameters for two time

Table 1: Rotational Diffusion Parameters[a] and Average Relaxation Parameters[b] of IRS-PTB in the Apo and Bound Forms

	400 μM samples		200 μM samples	
	apo	bound	apo	bound
no. of residues used to calculate diffusion tensor	79	64	63	59
τ_m (ns)	8.20 ± 0.06	7.85 ± 0.01	6.55 ± 0.05	6.81 ± 0.16
$D_\parallel/D_\perp$	1.16 ± 0.07	1.23 ± 0.11	1.20 ± 0.07	1.36 ± 0.17
θ (deg)	74 ± 10	73 ± 23	78 ± 9	66 ± 16
ϕ (deg)	168 ± 13	166 ± 21	184 ± 11	183 ± 17
no. of residues	75	75	74	74
R_1 (s^{-1})	1.51 ± 0.01	1.60 ± 0.11	2.03 ± 0.38	1.95 ± 0.40
R_2 (s^{-1})	11.38 ± 1.94	11.04 ± 2.14	9.29 ± 1.79	9.81 ± 1.84
NOE	0.75 ± 0.31	0.68 ± 0.23	0.68 ± 0.24	0.69 ± 0.22
R_2/R_1	7.54 ± 1.07	6.90 ± 1.31	4.71 ± 1.13	5.19 ± 1.22
η_{xy}	5.56 ± 1.20	6.06 ± 1.27	5.33 ± 1.16	6.21 ± 1.95
R_2/η_{xy}	2.12 ± 0.31	1.89 ± 0.49	1.79 ± 0.24	1.75 ± 0.89

[a] The parameters for all proteins were determined using an axially symmetric prolate diffusion tensor where τ_m is the overall correlation time defined as $\tau_m = (2D_\parallel + 4D_\perp)^{-1}$, where $D_\perp/D_\parallel$ is the ratio of the diffusion rate constants around unique and perpendicular axes of the diffusion tensor, and θ and ϕ are the Euler angles defining the position of the unique axis. Parameter values and errors are as reported by the program quadric_diffusion. [b] Relaxation data are reported as the average ± the standard deviation. Relaxation parameters were determined from paired data sets for 400 μM samples and 200 μM samples.

scales (S_f^2 and S_s^2) and τ_e for the slower time scale. The model best describing the internal dynamics of each backbone amide group was selected using ModelFree as previously described (*43*), and a final ModelFree calculation was executed in which all dynamics parameters were simultaneously optimized. Uncertainties in the dynamics parameters were obtained from 500 Monte Carlo simulations carried out with ModelFree.

Side chain indole NH order parameters (S^2) and internal correlation times (τ_e) were obtained by fitting the R_1 and NOE data to the standard model-free formalism (model 2 above) using the axially symmetric diffusion tensor obtained from the backbone data and a difference between the parallel and perpendicular components of the chemical shift tensor ($\sigma_\parallel - \sigma_\perp$) of −89 ppm (*44*). R_{ex} values reported are the differences between the observed R_2 values and the R_2 values back-calculated from fitted model-free parameters. Side chain methyl relaxation data were fit to the original version of the Lipari−Szabo model-free formalism (*38, 39, 45*) (model 2) using Matlab (The Mathworks, Inc.). Side chain methyl model-free calculations assumed isotropic rotational diffusion (see the Supporting Information) with the correlation times determined from analysis of the backbone amide relaxation data. The calculations used a quadrupolar coupling constant (e^2qQ/h) of 167 kHz (*46*). Uncertainties in the dynamics parameters were obtained from 500 Monte Carlo simulations.

The statistics used to compare parameters are the *z*-test (for comparisons between two residues in the two different forms of IRS-PTB) and the paired *z*-test (for comparisons between the distributions of parameters in the two forms) (*47*). The *p* value represents the probability that the difference between the two values (or two distributions) will occur randomly.

RESULTS

Observation of IRS-PTB Aggregation. To relate the new results to the previous dynamics study by Olejniczak et al. (*19*), we attempted to replicate the previous observations of backbone dynamics in the apo form and the phosphopeptide-bound form. The previous study was performed at a protein concentration of 1 mM, under which conditions we observed substantial precipitation. Therefore, we performed initial relaxation experiments using 400 μM protein samples. ^{15}N relaxation parameters were determined for 91 of 112 backbone amide groups in the apo form and 83 of 112 backbone amide groups in the peptide-bound form. The average ^{15}N relaxation values determined from the paired data sets of both proteins are given in Table 1. The average longitudinal relaxation rate constant, R_1, is lower in the apo form than in the bound form, whereas the average transverse relaxation rate constant, R_2, and the average ratio R_2/R_1 are both lower in the bound form. Lower R_2/R_1 ratios imply faster tumbling for the complex. Thus, the observed differences are opposite from those anticipated considering that the bound form is expected to have a slightly higher effective molecular weight than the apo form.

The rotational diffusion tensors for IRS-PTB in the apo and bound forms were calculated from the R_2/R_1 ratios of appropriate amide groups. A statistically significant improvement in fit of the axially symmetric diffusion model relative to the isotropic model ($F_{exp} > F_{0.95}$) was observed for both forms, while there was no significant improvement in fit for the fully anisotropic model compared with the axially symmetric model ($F_{exp} < F_{0.95}$). A comparison of χ^2 goodness-of-fit parameters indicated that prolate axially symmetric diffusion tensors fit the data better than oblate axially symmetric tensors for both apo and peptide-bound forms of IRS-PTB. The resulting τ_m values were 8.20 ± 0.06 and 7.85 ± 0.01 ns for the apo and bound forms, respectively; other diffusion tensor parameters were the same within experimental error (Table 1). The observation of a longer rotational correlation time in the apo form compared with that of the bound form, along with the difference in R_1 and R_2 values noted above, suggests that the apo form of the domain undergoes self-association at a concentration of 400 μM. For this reason, new relaxation data sets were recorded for both apo and bound forms of the protein at concentrations of 200 μM. Comparisons of the 200 and 400 μM data later suggested that the bound sample at 400 μM may also have been affected by some self-association (vide infra).

Elimination of IRS-PTB Aggregation. ^{15}N relaxation data were collected for 89 of 112 backbone amide groups in a

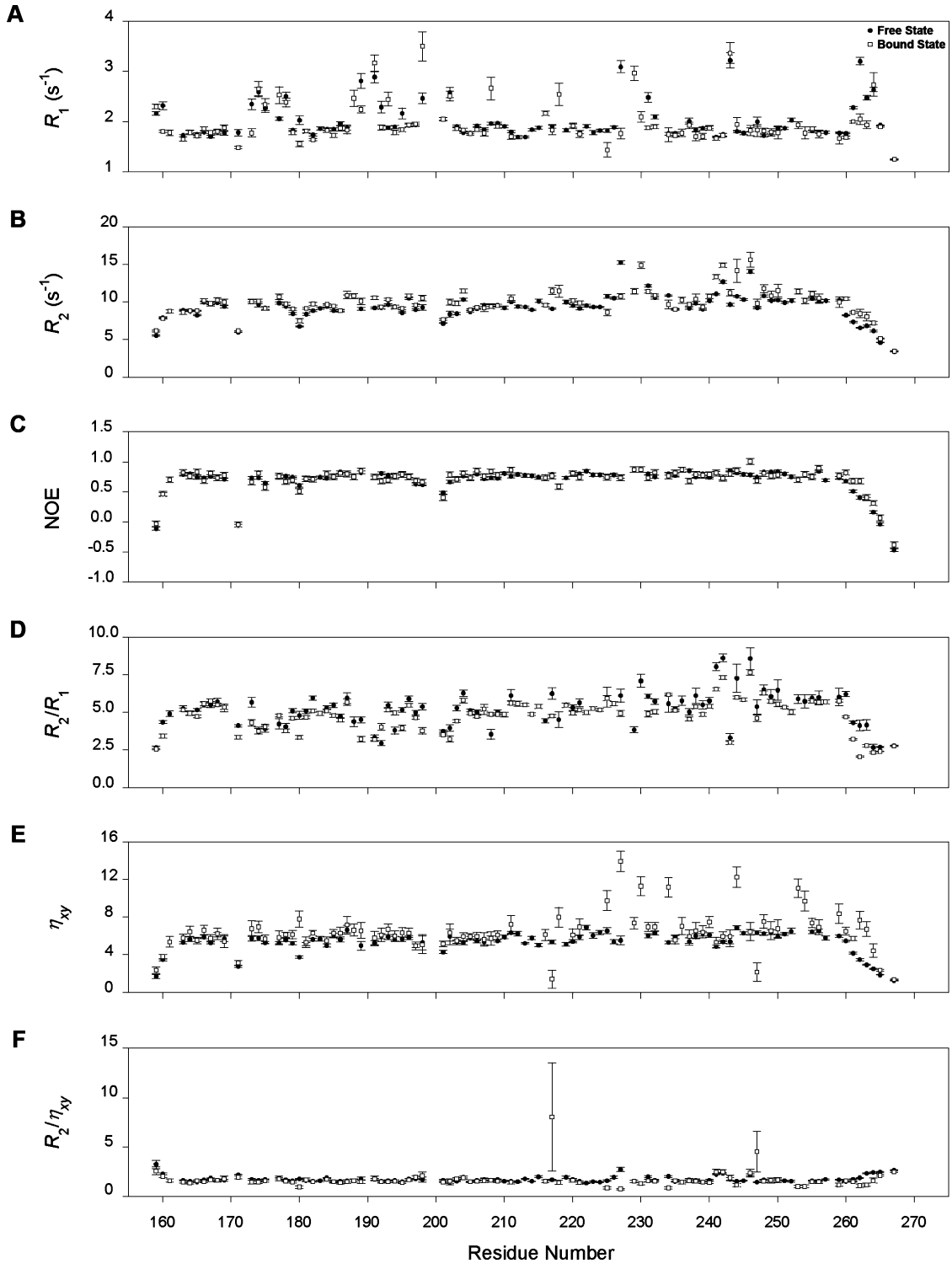

FIGURE 1: Plots of backbone amide relaxation parameters (A) R_1, (B) R_2, (C) NOE, (D) R_2/R_1, (E) η_{xy}, and (F) R_2/η_{xy} for 200 μM IRS-PTB in the apo (●) and bound (□) forms as a function of residue number.

200 μM sample of IRS-PTB in the apo form and 83 of 112 backbone amide groups in a 200 μM sample of the domain in the bound form. The R_1, R_2, NOE, R_2/R_1, and R_2/η_{xy} values for both proteins are plotted in Figure 1 and listed in the Supporting Information. The average values of relaxation parameters determined from the paired data sets of both proteins are given in Table 1. In contrast to that of the 400 μM sample, the average R_1 value in the 200 μM sample of peptide-bound IRS-PTB is lower than that in the free form, whereas the average R_2 value and the average R_2/R_1 ratio are both higher in the bound form. This trend is now consistent with the slightly increased molecular weight expected in the bound state.

The relaxation data for the 200 μM samples of IRS-PTB in apo and bound forms were best represented by a prolate axially symmetric diffusion tensor. The four parameters (τ_m, $D_\parallel/D_\perp$, θ, and ϕ) defining the axial prolate diffusion tensor for each domain are listed in Table 1. At the lower protein concentration, the τ_m value for the bound form (6.81 $\pm$ 0.16 ns) is slightly higher than that of the free form (6.55 $\pm$ 0.05 ns). This observation is also consistent with the expectation that an increase in molecular weight due to peptide binding

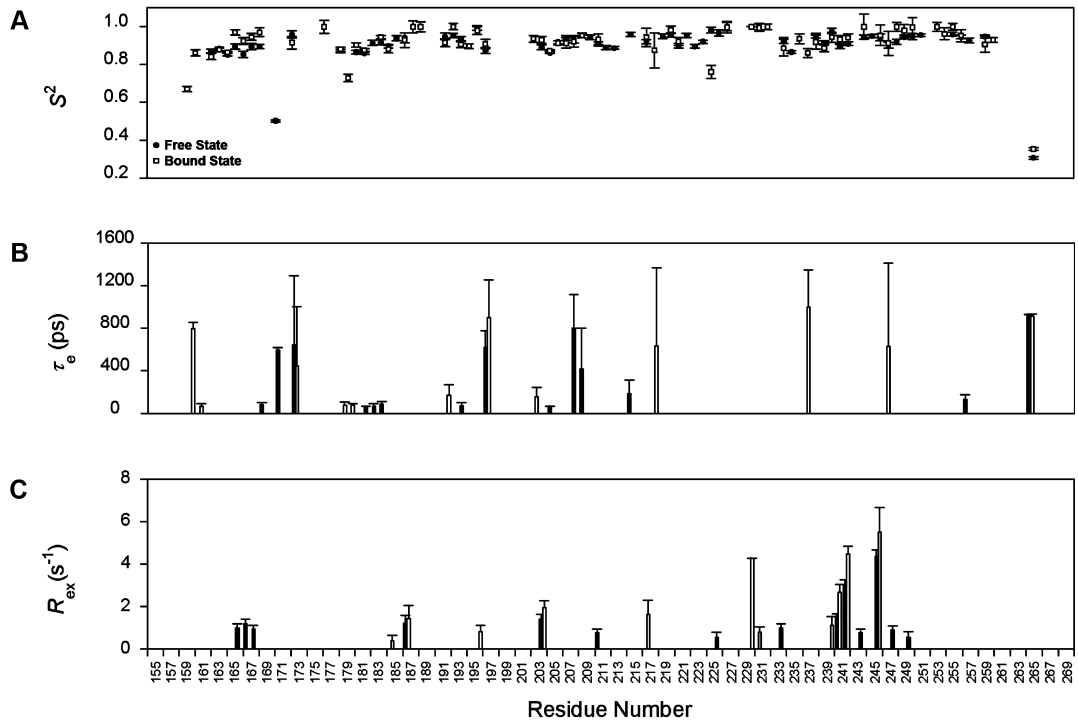

FIGURE 2: Plots of backbone amide dynamics parameters (A) S^2, (B) τ_e, and (C) R_{ex}, for 200 μM IRS-PTB in the apo (● and black bars) and bound (□ and white bars) forms as a function of residue number. Data are excluded for residues that were fit to model 5 and/or gave model-free SSE (sums of squared errors) values exceeding 20.

should result in a minor increase in overall rotational correlation time. Furthermore, the τ_m values observed for the 200 μM samples are consistent with the monomer molecular weight of IRS-PTB (12.6 kDa). Thus, diluting the samples from 400 to 200 μM appears to have been sufficient to alleviate most of the self-association observed at the higher concentration.

For each form of the protein, the majority of R_1, R_2, and NOE values are tightly clustered around the average value for that parameter (Figures 1A−C). However, there is a notable minority of R_1 values (approximately 30 and 24% of values in apo and bound states, respectively) that are substantially elevated above the expected range for proteins with the τ_m values determined here (Figure 1A). In theory, such elevated R_1 values can occur when internal motions occur on a nanosecond time scale, similar to that of the molecular rotation. Considering that the residues exhibiting elevated R_1 values are located in loops and terminal regions, we suspect that they are subject to segmental motions on the nanosecond time scale that are essentially independent of the core of the domain. Importantly, these are different from the residues showing significant changes in dynamics between free and bound forms (vide infra).

Backbone Amide Dynamics Parameters. Using the rotational diffusion tensors determined for apo and bound forms of IRS-PTB, the dynamics of backbone amide bond vectors were determined by fitting ^{15}N relaxation data for each vector to one of five versions of to the Lipari−-Szabo model-free formalism (*38*−*42*) commonly termed models 1−5. Model-free analysis yields three basic dynamics parameters describing the internal motions of each backbone amide bond vector: the generalized order parameter S^2, which is a measure of the degree of spatial restriction of the vector's motion (an S^2 of 0 indicates completely unrestricted motions, and an S^2 of 1 indicates completely restricted motions); the effective internal correlation time τ_e, which is a measure of the time scale of vector motion; and R_{ex}, which is a measure of conformational exchange on a microsecond to millisecond time scale.

Table 2: Average Dynamics Parameters of Backbone Amides in 200 μM IRS-PTB in the Apo and Bound Forms[a]

	apo	bound
S^2	0.912 ± 0.097	0.919 ± 0.096
τ_e (ps)	76 ± 214	64 ± 208
R_{ex} (s^{-1})	0.38 ± 0.84	0.42 ± 1.12

[a] Dynamics data reported as the average ± the standard deviation.

Of the backbone amide groups included in the model-free analyses of IRS-PTB, relaxation data for the majority (55 of 89 and 55 of 83 amide bond vectors in the apo and bound forms, respectively) were adequately fit to model 1 (S^2 only) or model 2 (S^2 and τ_e). Model 3, which includes the R_{ex} parameter, was invoked to satisfy relaxation data for 14 residues in the apo form and 11 residues in the bound form of the domain. The remaining residues could be fit only by incorporating a second time scale of internal motion as described by model 5 or could not be appropriately fit to any model. The dynamics data presented and discussed herein do not include residues that fall into the latter two categories because the parameters obtained from the model fitting may not be a reliable representation of the true dynamics of these residues. The S^2, τ_e, and R_{ex} values for the 200 μM samples of IRS-PTB in the apo and bound forms are plotted in Figure 2 and listed in the Supporting Information. The average dynamics parameters determined from the paired data sets of both proteins (Table 2) are similar in the free and bound states.

Side Chain Methyl Relaxation Parameters. To characterize the side chain motions within the apo and phosphopeptide-bound forms of IRS-PTB, we measured the relaxation of

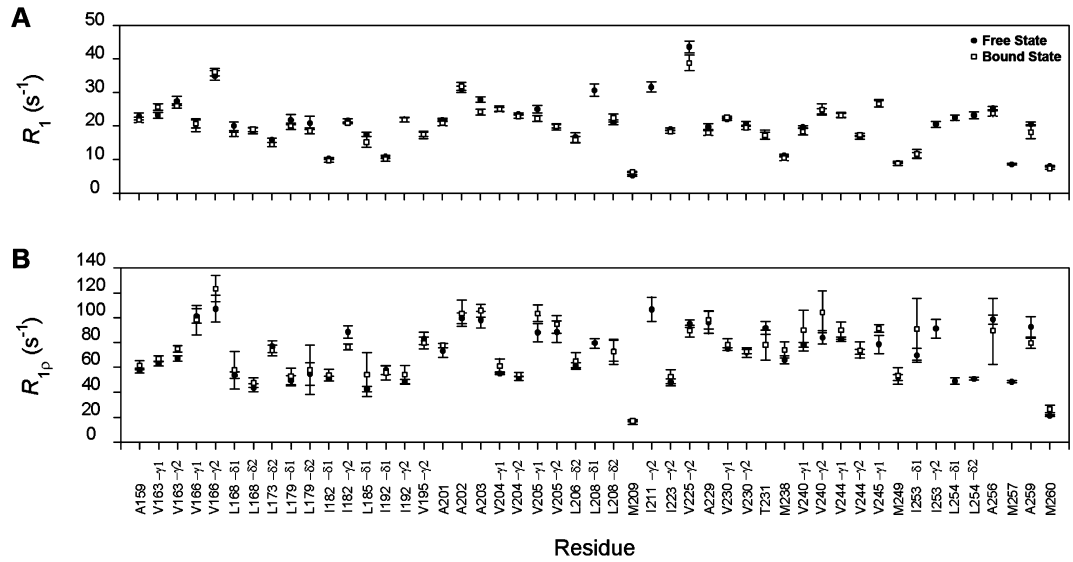

FIGURE 3: Plots of side chain methyl group relaxation parameters (A) R_1 and (B) $R_{1\rho}$ for IRS-PTB in the apo (●) and bound (□) forms as a function of residue number.

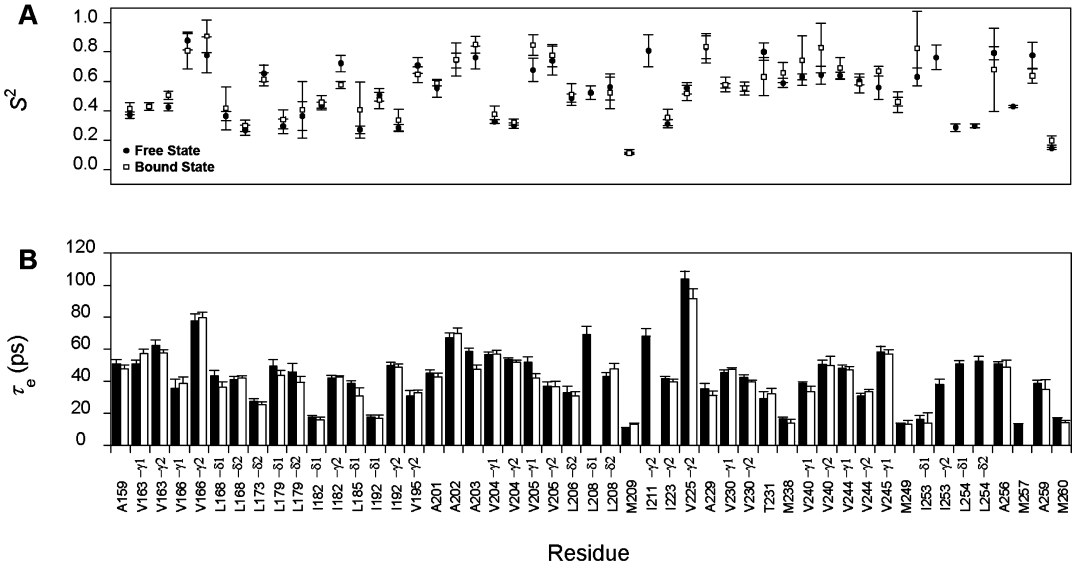

FIGURE 4: Plots of side chain methyl group dynamics parameters (A) S^2 and (B) τ_e for IRS-PTB in the apo (● and black bars) and bound (□ and white bars) forms as a function of residue number.

deuterium nuclei in side chain methyl groups (CH_2D). ^2H longitudinal (R_1) and transverse ($R_{1\rho}$) relaxation rates were determined for 49 of 71 side chain methyl groups in the apo form and 43 of 71 side chain methyl groups in the bound form of IRS-PTB. Relaxation parameters were not determined for a number of methyl groups in both proteins due to absent resonance peaks, partial or complete spectral overlap, or ambiguous assignments. The R_1 and $R_{1\rho}$ values for both forms are plotted in Figure 3 as a function of residue number and listed in the Supporting Information. The two forms of IRS-PTB display similar patterns of longitudinal and transverse relaxation across the protein sequence.

Side Chain Methyl Dynamics Parameters. The dynamics of side chain methyl groups in IRS-PTB in the apo and bound forms were determined by fitting ^2H relaxation data to the original version of the Lipari−Szabo model-free formalism (*38, 39*) using an isotropic diffusion tensor and the rotational correlation times determined from ^{15}N relaxation data for each protein. Use of an isotropic diffusion tensor for IRS-PTB is appropriate because the ^2H relaxation parameters are insensitive to the orientation of the methyl groups relative to the molecular rotational diffusion tensor; this was demonstrated by simulations of the relaxation parameters for the axially symmetric diffusion tensor of IRS-PTB (see the Supporting Information). Order parameters and effective correlation times were determined for 49 of 71 side chain methyl groups in the apo form and 43 of 71 side chain methyl groups in the bound form of IRS-PTB. The S_{axis}^2 and τ_e values are plotted as a function of residue number in Figure 4 and provided in the Supporting Information. In general, there are minimal differences between dynamics parameters for a particular residue in the apo and bound forms. However, there are substantial differences among the dynamics parameters of different residues in the same form of the protein.

Tryptophan Side Chain Relaxation and Dynamics. IRS-PTB contains two tryptophan residues (Trp-164 and Trp-237). The relaxation parameters for the side chain indole NH groups of these residues were obtained from the same experiments as the backbone amide relaxation parameters. The R_2 values of both residues in both states of the protein

Table 3: Relaxation Parameters of Tryptophan Side Chain Indole NH Groups in 200 μM IRS-PTB in the Apo and Bound Forms

	Trp-164		Trp-237	
	apo	bound	apo	bound
R_1 (s^{-1})	1.48 ± 0.03	1.71 ± 0.07	1.49 ± 0.02	1.51 ± 0.04
R_2 (s^{-1})	8.69 ± 0.12	8.35 ± 0.13	9.09 ± 0.12	9.06 ± 0.12
NOE	0.79 ± 0.03	0.70 ± 0.05	0.76 ± 0.03	0.72 ± 0.05
S^2	0.904 ± 0.017	0.659 ± 0.081	0.918 ± 0.014	0.889 ± 0.036
τ_e (ps)	59 ± 19	1579 ± 526	102 ± 36	257 ± 248
R_{ex} (s^{-1})	1.32 ± 0.20	2.11 ± 0.37	1.49 ± 0.18	1.72 ± 0.28

are higher than the theoretical limit for the standard model-free formalism (models 1 and 2), indicating that these groups experience conformational exchange broadening. Consequently, the data for the Trp indole groups were fit to model 4, yielding S^2, τ_e, and R_{ex} parameters. Table 3 lists the relaxation and dynamics parameters for these groups in both apo and bound forms of IRS-PTB. The order parameter of the Trp-237 side chain is similar in both forms of IRS-PTB, but the order parameter of the Trp-164 side chain decreases substantially from 0.90 ± 0.02 to 0.66 ± 0.08 upon phosphopeptide binding.

DISCUSSION

We have reported here backbone amide and side chain methyl group dynamics for IRS-PTB, in the apo form and the peptide-bound form. We compare the backbone dynamics in both forms with those previously reported at a higher protein concentration, and we discuss the influence of peptide binding on the mobility of backbone amides as well as side chain methyl groups in the protein domain.

Comparison of Backbone Dynamics with a Previous Study. There are several notable differences between the backbone amide dynamics reported in this study and those previously reported by Olejniczak and colleagues at a protein concentration of 1 mM (*19*). A majority of residues in the previous study were fit to a version of the model-free formalism that included an R_{ex} term. The requirement for R_{ex} terms to adequately fit the experimental data could arise from the presence of conformational exchange (in the microsecond to millisecond time regime) throughout the protein domain. However, an alternative possibility is that the actual rotational motion of the domain is slower than the correlation time (τ_m value) used in the model-free calculations. Olejniczak et al. did not report details of the method used for determination of rotational correlation times for the PTB in the free and bound states. However, they obtained τ_m values of 6.4 ± 0.5 and 6.8 ± 0.5 ns for the free and bound states, respectively, from data collected at a protein concentration of 1 mM. It is noteworthy that our data collected at 400 μM yielded substantially higher τ_m values (based upon ratios of R_2 to R_1 values) and that we observed τ_m values comparable to those from the previous study only at a lower concentration (200 μM). Therefore, the discrepancy between current and previous results may be due to protein aggregation that was not identified in the previous study. It is important to point out that collection of data at a concentration of 200 μM was made possible by the relatively recent innovation of cryogenically cooled NMR probes, which were not widely available at the time of the previous study. In addition to the difference in R_{ex} values, order parameters for a number of residues differ between the previously reported data and those reported herein. Considering the differences in τ_m values and R_{ex} terms discussed above, such differences in order parameters are perhaps not surprising and could be indirectly attributed to differences in the aggregation state of the protein.

Changes in Protein Mobility Induced by Peptide Binding. The average order parameters for IRS-PTB in the apo and bound forms are the same within error, 0.912 ± 0.097 for the apo form and 0.919 ± 0.096 for the bound form (average of the values of 49 equivalent positions ± the standard deviation); these distributions do not differ significantly ($p = 0.70$ in a paired z-test). Nevertheless, pairwise comparisons of order parameters for individual residues (Figure 5) identified 14 residues whose order parameters differ between the two proteins at the ≥90% confidence level (listed in Table 4).

Similarly, the distributions of side chain methyl group dynamics parameters for IRS-PTB are not significantly different between the apo and bound forms; average (±standard deviation) S_{axis}^2 values are 0.54 ± 0.20 for the apo form and 0.56 ± 0.19 for the bound form ($p = 0.57$ in a paired z-test; $n = 43$), whereas average τ_e values are 42 ± 18 ps for the apo form and 40 ± 18 ps for the bound form ($p = 0.63$ in a paired z-test; $n = 43$). Pairwise comparisons of individual residues reveal only three residues whose side chain order parameters differ significantly between the two forms of IRS-PTB; these are listed in Table 5.

Figure 6 shows the structure of IRS-PTB, highlighting the residues whose backbone amide chemical shifts change upon phosphopeptide binding (panels A and B) and those whose backbone or side chain order parameters change upon binding (panels C−G). Although X-ray structures have been reported for both the apo and phosphopeptide-bound forms of IRS-PTB (*18*), the coordinates of these X-ray structures are not available. Nevertheless, chemical shift changes observed in the course of this study provide an indication of local structural differences between the two forms in regions of the domain not in direct contact with the bound peptide. The backbone amide chemical shift changes are generally localized in the long, C-terminal α-helix that lies approximately parallel to the bound peptide. However, there is also a band of chemical shift changes extending across the front face of the β-sandwich (Figure 6A), suggesting that peptide binding induces minor structural adjustments in this side of the sheet. Of those residues displaying a change in backbone mobility upon peptide binding, only five residues are located in the regions that display changes in backbone chemical shift. Four of these residues, Asn-248, Glu-255, Met-260, and Arg-265, are all located in the C-terminal α-helix but are separated from the bound peptide by 2.0−8.4 Å, suggesting that the decreased flexibility of these residues can be attributed to direct or indirect interactions of the helix with the bound peptide. The fifth residue, Val-225 (red in Figure 6C), is located on the front face of the β-sheet, 5.0 Å from the bound peptide, and exhibits the most dramatic change in backbone flexibility between the apo and bound forms of the domain ($\Delta S^2 = -0.222 \pm 0.037$; $p < 0.01$). Importantly, the amide resonance of Val-225 is well-resolved in the HSQC spectrum (see the Supporting Information), and the relaxation decay curves are of high quality (Figure 7). Both R_1 and R_2 relaxation rates are clearly lower in the bound state than in the apo state, consistent with the calculated decrease in order

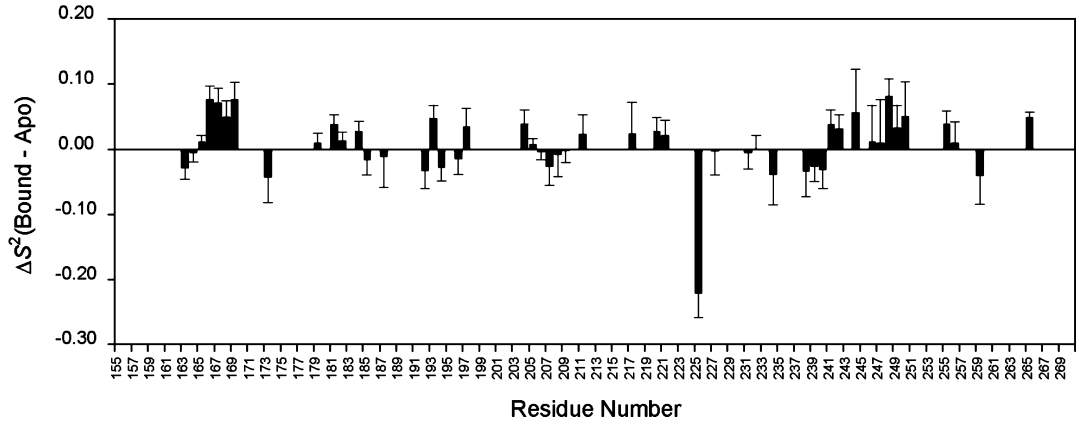

FIGURE 5: Differences between backbone amide S^2 values in the free and bound forms of IRS-PTB as a function of residue number.

Table 4: Residues Exhibiting a Significant Change in Backbone Amide Order Parameters between the Apo and Bound Forms of IRS-PTB

residue	structural location	ΔS^2 (bound − apo)	error in ΔS^2	p value[a]
163	β-strand 1	−0.029	0.018	0.10
166	β-strand 1	0.076	0.021	<0.01
167	β-strand 1	0.071	0.023	<0.01
168	β-strand 1	0.049	0.026	0.06
169	$\beta1-\beta2$ loop	0.076	0.027	<0.01
181	β-strand 2	0.038	0.015	0.01
184	β-strand 2	0.027	0.016	0.09
193	β-strand 3	0.047	0.020	0.02
204	β-strand 4	0.039	0.022	0.07
225	β-strand 6	−0.222	0.037	<0.01
241	$\beta7-\alpha1$ loop	0.038	0.022	0.08
248	α-helix 1	0.081	0.027	<0.01
255	α-helix 1	0.039	0.020	0.05
265	C-terminus	0.048	0.009	<0.01

[a] p value based on a z-test.

Table 5: Residues Exhibiting a Significant Change in Side Chain Methyl Group Dynamics Parameters between the Apo and Bound Forms of IRS-PTB

residue	structural location	ΔS_{axis}^2 (bound − apo)	error in ΔS_{axis}^2	p value[a]
Val-163-$\gamma2$	β-strand 1	0.080	0.037	0.03
Ile-182-$\gamma2$	β-strand 2	−0.145	0.062	0.02
Met-260	α-helix 1	0.057	0.030	0.06

[a] p value based on a z-test.

parameter (increase in flexibility). The mechanism by which binding of the phosphopeptide enhances the flexibility of Val-225 is not directly indicated by these data. However, it is noteworthy that Val-225 is adjacent to Arg-227, which interacts directly with the phosphotyrosine of the bound peptide. Although dynamics data are not available for Arg-227, it seems plausible that structural adjustment of Arg-227 to accommodate interaction with the peptide results in a decreased level of packing interactions with Val-225, thus allowing an increased level of motion of Val-225.

The remaining residues that demonstrate significant changes in dynamics are all located remotely from the bound peptide (Figure 6C−F); distances to the peptide range from 10.8 Å (Lys-169) to 19.6 Å (Ile-182). However, it is striking that 11 of these 12 residues are clustered together, forming a network of interactions with interresidue contacts of ≤4 Å. This network is represented schematically in Figure 6G. Most of the residues are located in the β-sheet at the back of the structure in Figure 6C,E (front in Figure 6D,F). This is the opposite face of the β-sandwich from the chemical shift changes (Figure 6A,B). Furthermore, many of the residues are buried, contributing to the hydrophobic core of the domain (Figure 6E,F). The precise mechanism by which the effect of peptide binding is transmitted to this cluster of remote residues is not directly indicated by these data. One possibility is that the structural and dynamical changes surrounding Val-225 influence the packing interactions with the opposite β-sheet (close to Val-204) and that these changes are propagated to the other residues through the series of interactions depicted in Figure 6G. An alternative is that structural changes due to peptide binding cause rigidification of Asn-248 and that the change at Asn-248 allows an increased level of motion of Trp-164, which forms a node for interactions with the other residues in the remote network. In either of these cases, the dynamics of each residue could be influenced either by small structural adjustments of nearby residues or directly by the movements of nearby residues (if dynamical coupling exists). Irrespective of the precise mechanism, the data indicate that dynamical measurements are sensitive to the presence of interaction networks, even when structural changes are extremely subtle.

It is interesting to consider possible ways that the proposed network of interactions can be further investigated. One approach would be to mutate residues at the peptide end of the network (e.g., Val-225 or Asn-248) to determine whether these influence the propagation of dynamics changes to remote residues. A complementary approach would be to modify remote residues (e.g., Lys-169 or Arg-184) and then to determine whether the changes affect the properties of the residues close to the peptide binding site or the affinity, enthalpy, or entropy of peptide binding. To probe the interactions of specific pairs of residues in the network, it may be useful to perform double mutant cycle analyses; nonadditive influences of the mutations on protein stability or ligand binding would provide evidence of direct or indirect interactions. Further evidence of an interaction network may be able to be obtained using the dynamics covariation method (*48, 49*), in which dynamics parameters are measured for several mutants and the variations at each position are correlated with those at each other position to identify pairs whose dynamics are influenced by similar factors. Finally, molecular dynamics simulations are expected to be helpful in complementing the experiments presented here and proposed experiments and providing mechanistic insights into the propagation of dynamics changes across IRS-PTB.

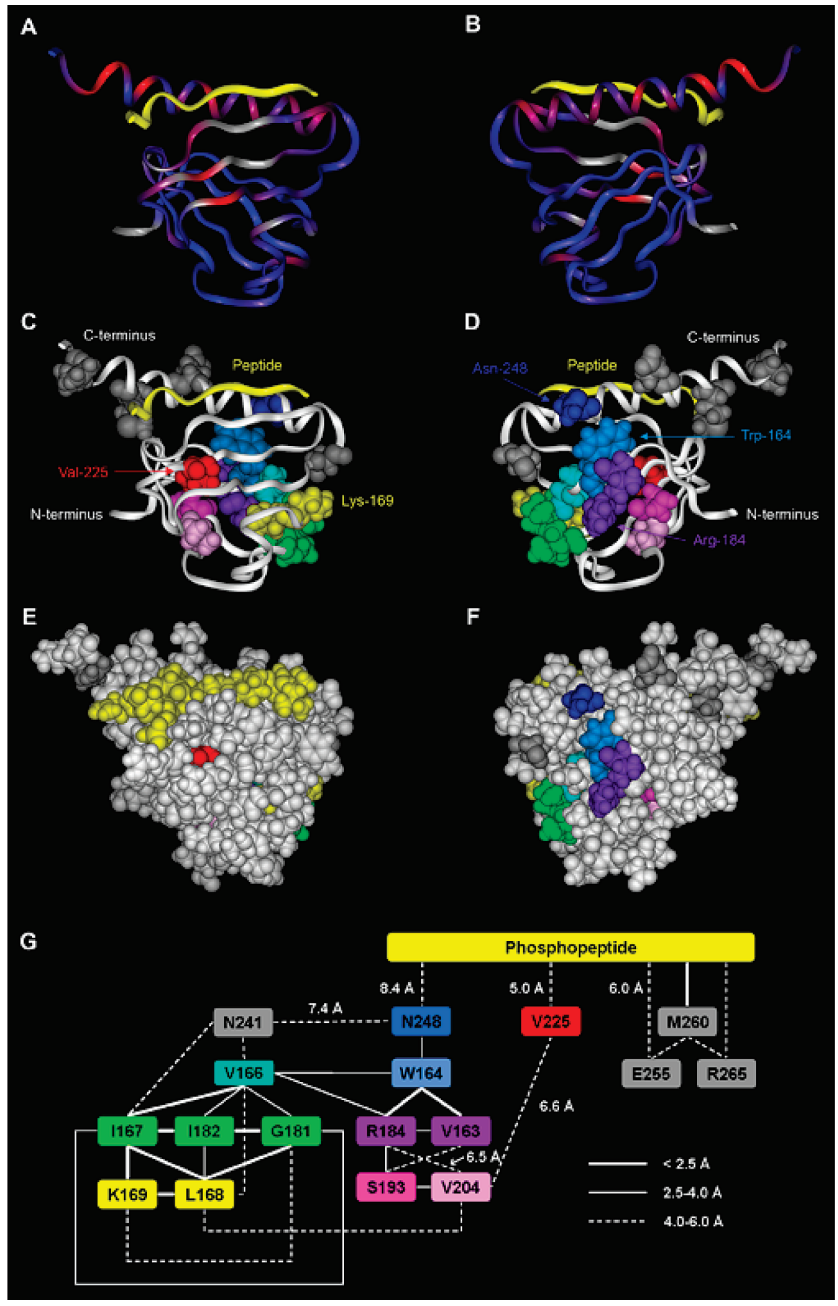

FIGURE 6: (A, C, and E) Front and (B, D, and F) back views of IRS-PTB bound to a phosphopeptide derived from the IL-4 receptor (PBD entry 1IRS) and color-coded to show changes in amide chemical shift and fast time scale dynamics between the apo and bound states. (A and B) Ribbon structure colored according to the change ($\Delta\delta_{bb}$) in backbone NH group chemical shift, defined as $\Delta\delta_{bb} = |\Delta\delta_{HN}| + 0.2|\Delta\delta_{N}|$, where $\Delta\delta_{HN}$ and $\Delta\delta_{N}$ are the changes in $^{1}H_{N}$ and $^{15}N_{H}$ chemical shifts between the apo and bound states, respectively. The coloring scheme is on a continuous scale from blue to red, corresponding to $\Delta\delta_{bb}$ values of 0−0.30. The ribbon structure of the bound phosphopeptide is colored yellow. Residues for which chemical shift data were not available in one or both states are colored gray. (C and D) Residues whose backbone amide groups and side chain methyl groups display a significant change in order parameter are shown in space-filling representation and colored to highlight the proposed network of long-range dynamical changes. The phosphopeptide is shown in space-filling representation and colored yellow. (E and F) Same views as panels C and D, respectively, with all atoms shown in space-filling representation. (G) Schematic representation of the network of dynamical communication with residues labeled and color-coded with the same colors as in panels C−F. Lines between residues indicate the interresidue distances (thick lines, <2.5 Å; thin lines, 2.5−4.0 Å; broken lines, 4.0−6.0 Å unless otherwise indicated).

Concluding Remarks. The dynamics data presented herein indicate that binding of a phosphopeptide to one surface of IRS-PTB gives rise to changes in backbone and side chain flexibility at positions remote from the peptide binding site. Considering that the majority of these remote residues are clustered together in the same region of the structure, it appears likely that they form a network of mutually dependent (cooperative) interactions and that this network is coupled to the peptide binding site through intervening residues. Interestingly, the phospholipid binding site previously proposed for IRS-PTB (*16*) includes Lys-169, which is located at the end of the dynamical network most distant from the phosphopeptide. It is therefore tempting to speculate that the network could serve as a coupling mechanism between the phosphopeptide and putative phospholipid binding sites. Notably, changes in protein dynamics similar to those observed here were observed previously upon binding of a peptide to a PDZ domain (*7*), and these changes were in

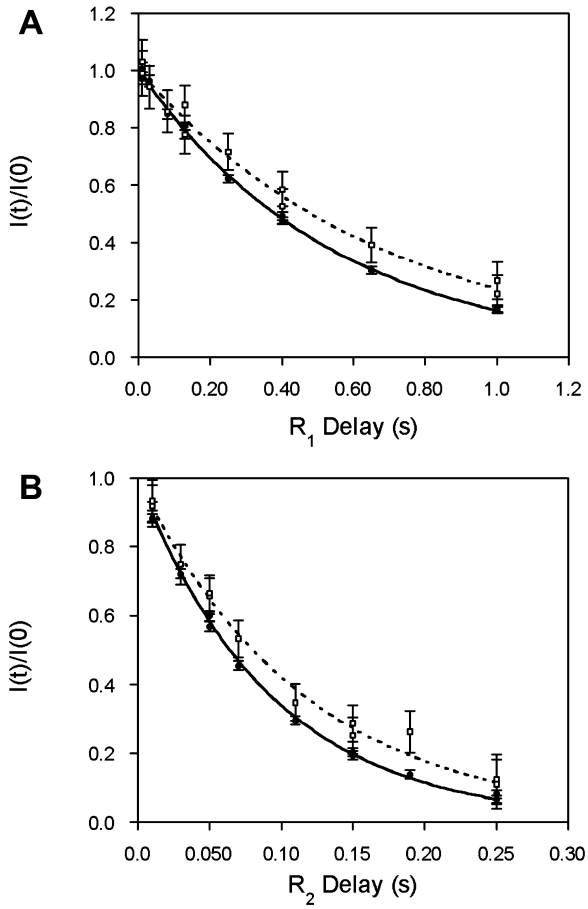

FIGURE 7: Plots of Val-225 backbone amide (A) R_1 and (B) R_2 relaxation decays for IRS-PTB in the apo (● and solid lines) and bound (□ and dotted lines) forms. Peak intensities at each time point, $I(t)$, were normalized by dividing $I(t)$ by the initial intensity, $I(0)$; error bars were obtained by dividing the error in $I(t)$ by $I(0)$. The R_1, R_2, and NOE values are 1.82 ± 0.04 s^{-1}, 10.80 ± 0.25 s^{-1}, and 0.75 ± 0.02 in the apo state and 1.44 ± 0.14 s^{-1}, 8.64 ± 0.44 s^{-1}, and 0.74 ± 0.05 in the bound state, respectively.

accord with interactions predicted by statistical coupling analysis (*10*). In the case of PDZ domains, the coupling was proposed to influence binding of the remote residues to adaptor proteins (*7*). Thus, the presence of dynamical coupling networks may be an emerging paradigm among multifunctional signaling domains.

ACKNOWLEDGMENT

We thank David Smiley (Indiana University) and Yvonne Brede for synthesis of the phosphopeptide, Drs. Douglas E. Brown and John W. Tomaszewski (Indiana University NMR Facility) and Dr. Ming-Ming Zhou (Mt. Sinai School of Medicine, New York, NY) for helpful discussions, and Drs. Lewis Kay (University of Toronto, Toronto, ON), Mark Rance (University of Cincinnati, Cincinnati, OH), and Josh Wand (University of Pennsylvania, Philadelphia, PA) for providing pulse programs.

SUPPORTING INFORMATION AVAILABLE

Protein sequence of the IRS-PTB construct, eight tables containing the backbone amide and side chain methyl group relaxation and model-free dynamics data for IRS-PTB, assigned ^{15}N and methyl ^{13}C HSQC spectra for IRS-PTB, and figures, methods, and discussion for simulations of the ^{2}H relaxation parameters for the axially symmetric diffusion tensor of IRS-PTB. This material is available free of charge via the Internet at http://pubs.acs.org.

REFERENCES

1. Rajagopalan, P. T., Lutz, S., and Benkovic, S. J. (2002) Coupling interactions of distal residues enhance dihydrofolate reductase catalysis: Mutational effects on hydride transfer rates. *Biochemistry 41*, 12618–12628.
2. Liebeton, K., Zonta, A., Schimossek, K., Nardini, M., Lang, D., Dijkstra, B. W., Reetz, M. T., and Jaeger, K. E. (2000) Directed evolution of an enantioselective lipase. *Chem. Biol. 7*, 709–718.
3. Gregoret, L. M., and Sauer, R. T. (1993) Additivity of mutant effects assessed by binomial mutagenesis. *Proc. Natl. Acad. Sci. U.S.A. 90*, 4246–4250.
4. Green, S. M., and Shortle, D. (1993) Patterns of nonadditivity between pairs of stability mutations in staphylococcal nuclease. *Biochemistry 32*, 10131–10139.
5. Istomin, A. Y., Gromiha, M. M., Vorov, O. K., Jacobs, D. J., and Livesay, D. R. (2008) New insight into long-range nonadditivity within protein double-mutant cycles. *Proteins 70*, 915–924.
6. Rod, T. H., Radkiewicz, J. L., and Brooks, C. L., III (2003) Correlated motion and the effect of distal mutations in dihydrofolate reductase. *Proc. Natl. Acad. Sci. U.S.A. 100*, 6980–6985.
7. Lockless, S. W., and Ranganathan, R. (1999) Evolutionarily conserved pathways of energetic connectivity in protein families. *Science 286*, 295–299.
8. Socolich, M., Lockless, S. W., Russ, W. P., Lee, H., Gardner, K. H., and Ranganathan, R. (2005) Evolutionary information for specifying a protein fold. *Nature 437*, 512–518.
9. Russ, W. P., Lowery, D. M., Mishra, P., Yaffe, M. B., and Ranganathan, R. (2005) Natural-like function in artificial WW domains. *Nature 437*, 579–583.
10. Fuentes, E. J., Der, C. J., and Lee, A. L. (2004) Ligand-dependent dynamics and intramolecular signaling in a PDZ domain. *J. Mol. Biol. 335*, 1105–1115.
11. Clarkson, M. W., and Lee, A. L. (2004) Long-range dynamic effects of point mutations propagate through side chains in the serine protease inhibitor eglin c. *Biochemistry 43*, 12448–12458.
12. Clarkson, M. W., Gilmore, S. A., Edgell, M. H., and Lee, A. L. (2006) Dynamic coupling and allosteric behavior in a nonallosteric protein. *Biochemistry 45*, 7693–7699.
13. White, M. F. (1994) The IRS-1 signaling system. *Curr. Opin. Genet. Dev. 4*, 47–54.
14. White, M. F. (2003) IRS-Protein Scaffolds and Insulin/IGF Action. In *Handbook of Cell Signaling*, pp 409−419, Academic Press, New York.
15. Uhlik, M. T., Temple, B., Bencharit, S., Kimple, A. J., Siderovski, D. P., and Johnson, G. L. (2005) Structural and evolutionary division of phosphotyrosine binding (PTB) domains. *J. Mol. Biol. 345*, 1–20.
16. Takeuchi, H., Matsuda, M., Yamamoto, T., Kanematsu, T., Kikkawa, U., Yagisawa, H., Watanabe, Y., and Hirata, M. (1998) PTB domain of insulin receptor substrate-1 binds inositol compounds. *Biochem. J. 334* (Part 1), 211–218.
17. Dhe-Paganon, S., Ottinger, E. A., Nolte, R. T., Eck, M. J., and Shoelson, S. E. (1999) Crystal structure of the pleckstrin homology-phosphotyrosine binding (PH-PTB) targeting region of insulin receptor substrate 1. *Proc. Natl. Acad. Sci. U.S.A. 96*, 8378–8383.
18. Eck, M. J., DhePaganon, S., Trub, T., Nolte, R. T., and Shoelson, S. E. (1996) Structure of the IRS-1 PTB domain bound to the juxtamembrane region of the insulin receptor. *Cell 85*, 695–705.
19. Olejniczak, E. T., Zhou, M. M., and Fesik, S. W. (1997) Changes in the NMR-derived motional parameters of the insulin receptor substrate 1 phosphotyrosine binding domain upon binding to an interleukin 4 receptor phosphopeptide. *Biochemistry 36*, 4118–4124.
20. Zhou, M. M., Huang, B. H., Olejniczak, E. T., Meadows, R. P., Shuker, S. B., Miyazaki, M., Trub, T., Shoelson, S. E., and Fesik, S. W. (1996) Structural basis for IL-4 receptor phosphopeptide recognition by the IRS-1 PTB domain. *Nat. Struct. Biol. 3*, 388–393.
21. Gasteiger, E., Hoogland, C., Gattiker, A., Duvaud, S., Wilkins, M. R., Appel, R. D., and Bairoch, A. (2005) Protein Identification and Analysis Tools on the ExPasy Server. In *The Proteomics Protocols Handbook* (Walker, J. M., Ed.) pp 571−607, Humana Press, Totowa, NJ.

22. Neri, D., Szyperski, T., Otting, G., Senn, H., and Wuthrich, K. (1989) Stereospecific nuclear magnetic resonance assignments of the methyl groups of valine and leucine in the DNA-binding domain of the 434 repressor by biosynthetically directed fractional ^{13}C labeling. *Biochemistry 28*, 7510–7516.
23. Grzesiek, S., and Bax, A. (1992) Correlating Backbone Amide and Side-Chain Resonances in Larger Proteins by Multiple Relayed Triple Resonance Nmr. *J. Am. Chem. Soc. 114*, 6291–6293.
24. Wittekind, M., and Mueller, L. (1993) Hncacb, A High-Sensitivity 3D Nmr Experiment to Correlate Amide-Proton and Nitrogen Resonances with the α-Carbon and β-Carbon Resonances in Proteins. *J. Magn. Reson., Ser. B 101*, 201–205.
25. Muhandiram, D. R., and Kay, L. E. (1994) Gradient-Enhanced Triple-Resonance 3-Dimensional Nmr Experiments with Improved Sensitivity. *J. Magn. Reson., Ser.B 103*, 203–216.
26. Zhang, O. W., Kay, L. E., Olivier, J. P., and Forman-Kay, J. D. (1994) Backbone ^{1}H and ^{15}N resonance assignments of the N-terminal Sh3 domain of Drk in folded and unfolded states using enhanced-sensitivity pulsed-field gradient NMR techniques. *J. Biomol. NMR 4*, 845–858.
27. Montelione, G. T., Lyons, B. A., Emerson, S. D., and Tashiro, M. (1992) An efficient triple resonance experiment using ^{13}C isotropic mixing for determining sequence-specific resonance assignments of isotopically-enriched proteins. *J. Am. Chem. Soc. 114*, 10974–10975.
28. Grzesiek, S., Anglister, J., and Bax, A. (1993) Correlation of backbone amide and aliphatic side-chain resonances in $^{13}C/^{15}N$-enriched proteins by isotropic mixing of ^{13}C magnetization. *J. Magn. Reson., Ser. B 101*, 114–119.
29. Bax, A., Clore, G. M., and Gronenborn, A. M. (1990) H-1-H-1 Correlation Via Isotropic Mixing of C-13 Magnetization, A New 3-Dimensional Approach for Assigning H-1 and C-13 Spectra of C-13-Enriched Proteins. *J. Magn. Reson. 88*, 425–431.
30. Bax, A., Delaglio, F., Grzesiek, S., and Vuister, G. W. (1994) Resonance assignment of methionine methyl groups and chi 3 angular information from long-range proton-carbon and carbon-carbon J correlation in a calmodulin-peptide complex. *J. Biomol. NMR 4*, 787–797.
31. Kay, L. E., Torchia, D. A., and Bax, A. (1989) Backbone dynamics of proteins as studied by ^{15}N inverse detected heteronuclear NMR spectroscopy: Application to staphylococcal nuclease. *Biochemistry 28*, 8972–8979.
32. Farrow, N. A., Muhandiram, R., Singer, A. U., Pascal, S. M., Kay, C. M., Gish, G., Shoelson, S. E., Pawson, T., Forman-Kay, J. D., and Kay, L. E. (1994) Backbone dynamics of a free and phosphopeptide-complexed Src homology 2 domain studied by ^{15}N NMR relaxation. *Biochemistry 33*, 5984–6003.
33. Kroenke, C. D., Loria, J. P., Lee, L. K., Rance, M., and Palmer, A. G. (1998) Longitudinal and transverse ^{1}H-^{15}N dipolar ^{15}N chemical shift anisotropy relaxation interference: Unambiguous determination of rotational diffusion tensors and chemical exchange effects in biological macromolecules. *J. Am. Chem. Soc. 120*, 7905–7915.
34. Muhandiram, D. R., Yamazaki, T., Sykes, B. D., and Kay, L. E. (1995) Measurement of ^{2}H T_1 and $T_{1\rho}$ relaxation times in uniformly ^{13}C-labeled and fractionally ^{2}H-labeled proteins in solution. *J. Am. Chem. Soc. 117*, 11536–11544.
35. Seewald, M. J., Pichumani, K., Stowell, C., Tibbals, B. V., Regan, L., and Stone, M. J. (2000) The role of backbone conformational heat capacity in protein stability: Temperature dependent dynamics of the B1 domain of *Streptococcal* protein G. *Protein Sci. 9*, 1177–1193.
36. Fushman, D., and Cowburn, D. (1998) Model-independent analysis of ^{15}N chemical shift anisotropy from NMR relaxation data. Ubiquitin as a test example. *J. Am. Chem. Soc. 120*, 7109–7110.
37. Bruschweiler, R., Liao, X. B., and Wright, P. E. (1995) Long-range motional restrictions in a multidomain zinc-finger protein from anisotropic tumbling. *Science 268*, 886–889.
38. Lipari, G., and Szabo, A. (1982) Model-free approach to the interpretation of nuclear magnetic resonance relaxation in macromolecules. 1. Theory and range of validity. *J. Am. Chem. Soc. 104*, 4546–4559.
39. Lipari, G., and Szabo, A. (1982) Model-free approach to the interpretation of nuclear magnetic resonance relaxation in macromolecules. 2. Analysis of experimental results. *J. Am. Chem. Soc. 104*, 4559–4570.
40. Clore, G. M., Driscoll, P. C., Wingfield, P. T., and Gronenborn, A. M. (1990) Analysis of the backbone dynamics of interleukin-1β using two-dimensional inverse detected heteronuclear ^{15}N-^{1}H NMR spectroscopy. *Biochemistry 29*, 7387–7401.
41. Clore, G. M., Szabo, A., Bax, A., Kay, L. E., Driscoll, P. C., and Gronenborn, A. M. (1990) Deviations from the simple 2-parameter model-free approach to the interpretation of ^{15}N nuclear magnetic-relaxation of proteins. *J. Am. Chem. Soc. 112*, 4989–4991.
42. Barbato, G., Ikura, M., Kay, L. E., Pastor, R. W., and Bax, A. (1992) Backbone dynamics of calmodulin studied by ^{15}N relaxation using inverse detected two-dimensional NMR spectroscopy: The central helix is flexible. *Biochemistry 31*, 5269–5278.
43. Mandel, A. M., Akke, M., and Palmer, A. G., III (1995) Backbone dynamics of *Escherichia coli* ribonuclease HI: Correlations with structure and function in an active enzyme. *J. Mol. Biol. 246*, 144–163.
44. Stone, M. J., Chandrasekhar, K., Holmgren, A., Wright, P. E., and Dyson, H. J. (1993) Comparison of Backbone and Tryptophan Side-Chain Dynamics of Reduced and Oxidized *Escherichia coli* Thioredoxin Using N-15 Nmr Relaxation Measurements. *Biochemistry 32*, 426–435.
45. Millet, O., Muhandiram, D. R., Skrynnikov, N. R., and Kay, L. E. (2002) Deuterium spin probes of side-chain dynamics in proteins. 1. Measurement of five relaxation rates per deuteron in ^{13}C-labeled and fractionally ^{2}H-enriched proteins in solution. *J. Am. Chem. Soc. 124*, 6439–6448.
46. Mittermaier, A., and Kay, L. E. (1999) Measurement of methyl ^{2}H quadrupolar couplings in oriented proteins. How uniform is the quadrupolar coupling constant? *J. Am. Chem. Soc. 121*, 10608–10613.
47. Moore, D. S., and McCabe, G. P. (2004) *Introduction to the Practice of Statistics*, W. H. Freeman and Company, New York.
48. Mayer, K. L., Earley, M. R., Gupta, S., Pichumani, K., Regan, L., and Stone, M. J. (2003) Covariation of backbone motion throughout a small protein domain. *Nat. Struct. Biol. 10*, 962–965.
49. Goehlert, V. A., Krupinska, E., Regan, L., and Stone, M. J. (2004) Analysis of side chain mobility among protein G B1 domain mutants with widely varying stabilities. *Protein Sci. 13*, 3322–3330.

BI801096B